AIP | Applied Physics Letters

Tailoring the surface plasmon resonance of embedded silver nanoparticles by combining nano- and femtosecond laser pulses

J. Doster, G. Baraldi, J. Gonzalo, J. Solis, J. Hernandez-Rueda, and J. Siegel

---

Articles you may be interested in
Surface plasmon resonance assisted rapid laser joining of glass
Appl. Phys. Lett. **105**, 083109 (2014); 10.1063/1.4894118

Localized surface plasmon of Ag nanoparticles affected by annealing and its coupling with the excitons of Rhodamine 6G
J. Vac. Sci. Technol. A **31**, 041401 (2013); 10.1116/1.4811819

Magneto-optical enhancement by surface plasmon resonance in magnetic "nano-onions" with multicore-shell structures
J. Appl. Phys. **97**, 10M514 (2005); 10.1063/1.1853206

Mega-electron-volt ion beam induced anisotropic plasmon resonance of silver nanocrystals in glass
Appl. Phys. Lett. **83**, 4137 (2003); 10.1063/1.1627936

Spectral narrowing of the emission from rhodamine 6G infiltrated in synthetic opals enhanced by the surface plasmon resonance
Appl. Phys. Lett. **83**, 2536 (2003); 10.1063/1.1615306

Tailoring the surface plasmon resonance of embedded silver nanoparticles by combining nano- and femtosecond laser pulses

J. Doster, G. Baraldi, J. Gonzalo, J. Solis, J. Hernandez-Rueda, and J. Siegel[a]
Laser Processing Group, Instituto de Optica, Serrano 121, 28006 Madrid, Spain

We demonstrate that the broad surface plasmon resonance (SPR) of a single layer of near-coalescence silver nanoparticles (NPs), embedded in a dielectric matrix can be tailored by irradiation with a single nanosecond laser pulse into a distribution featuring a sharp resonance at 435 nm. Scanning electron microscopy studies reveal the underlying mechanism to be a transformation into a distribution of well-separated spherical particles. Additional exposure to multiple femtosecond laser pulses at 400 nm or 800 nm wavelength induces polarization anisotropy of the SPR, with a peak shift that increases with laser wavelength. The spectral changes are measured *in-situ*, employing reflection and transmission micro-spectroscopy with a lateral resolution of 4 μm. Spectral maps as a continuous function of local fluence can be readily produced from a single spot. The results open exciting perspectives for dynamically tuning and switching the optical response of NP systems, paving the way for next-generation applications. © *2014 AIP Publishing LLC*. [http://dx.doi.org/10.1063/1.4871507]

The interaction of light with metal nanoparticles (NPs) triggers the collective oscillation of electrons at the NP surface, called surface plasmon resonance (SPR), which determines the optical response of the system. The SPR manifests itself as enhanced absorption within a certain spectral region, depending strongly on several parameters, including size, shape, and separation of the NPs, as well as the refractive index of the surrounding matrix.[1] While a constant SPR is adequate for standard applications, it constitutes an important limitation for advanced applications in which the optical response needs to be changed or switched between different states. While methods have been developed for modifying the size distribution[2,3] or even achieving shaping and alignment[4–6] of NP layers at substrate surfaces, post-processing of embedded NPs is complex because of the forces exerted by the surrounding medium.

Femtosecond (fs) laser pulses are capable for overcoming these forces. Using this approach spherical Ag NPs embedded in bulk glass have been reshaped into oblate or prolate spheroids with different aspect ratio,[7,8] or even nano-disks.[9] The shaping mechanism proposed by the authors involves field-driven electron emission at the poles of the NPs along the polarization axis. This process is accompanied by emission of Ag ions, which recombine with the trapped electrons to form elongated NPs.[10] It is worth noting that the estimated temperature increase after the initial shaping process is well above the melting point, leading to melting of the NPs,[11] which likely contributes to their smooth shape.

We have recently shown reshaping of non-spherical, near-coalescence Ag NPs embedded in an ultrathin dielectric film using off-resonant fs laser pulses.[12] A study of the light transmission spectrum at different laser spot positions showed a transformation from an isotropic SPR in the red to an anisotropic spectrum in the blue spectral region, featuring an intermediate regime of spectral bleaching caused by NP destruction.

In the present work, we introduce an all-laser-based approach for the fabrication of spherical or ellipsoidal, aligned Ag NPs that combines Pulsed Laser Deposition (PLD) for the initial formation of randomly shaped nano-structures with ns and fs laser irradiation to tailor the shape and alignment of the NPs. Initial ns irradiation leads to a pronounced isotropic SPR, while post-processing with on- and off-resonance fs laser pulses transforms it into an anisotropic SPR. Moreover, by combining reflection and transmission *in-situ* spectroscopy, we can extract the absorption spectrum, which is the most direct monitor of the SPR. The high spatial resolution of the setup and well-defined laser intensity distribution allows us to map the complete fluence dependence of the shaping process by analyzing a single laser spot.

Fig. 1 shows a sketch of the experimental setup developed for laser irradiation and *in-situ* high-resolution transmission and reflection spectroscopy. The sample was mounted on a three-axis motorized stage and irradiated by a focused laser beam, incident at 53° and derived from an amplified Ti:Sa laser amplifier operating at a wavelength $\lambda = 800$ nm. The laser output could be changed for the experiment to provide pulses 100 fs long, either at 800 nm (standard mode) or 400 nm. Moreover, by blocking the seed laser of the amplifier, pulses of 8 ns at 800 nm could be obtained. In all cases, the incident laser polarization was chosen to be *s*-polarized (along the y-axis) in order to set the polarization vector to lie within the surface plane. The spot size was inversely proportional to the diameter of the circular aperture near the laser head. The intensity distribution at the sample plane was measured to be nicely Gaussian using the method described in Ref. 13, demonstrating that the influence of the aperture is negligible at least up to radial distances larger than twice the spot radius. We used spot sizes (1/e^2 diameter) of 98.4 μm × 59.2 μm or 106.6 μm × 58.9 μm for irradiations at 400 nm and 800 nm, respectively.

An *in-situ* microscope with a 20× objective lens and a 200 mm tube lens (L1) was used for aiding sample irradiation
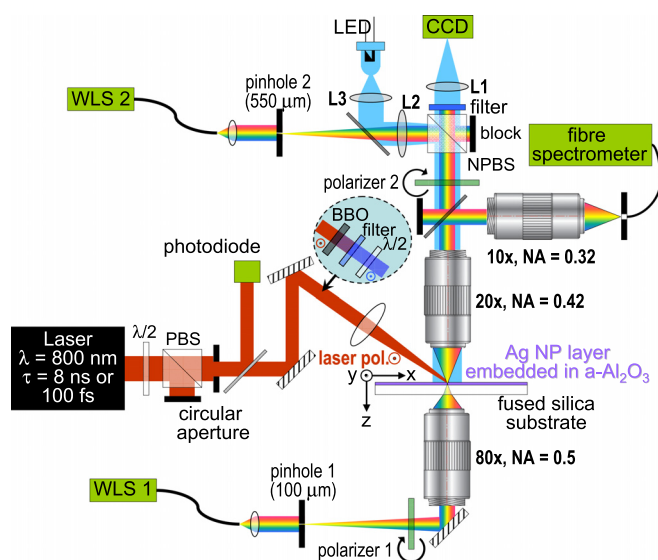
[a]E-mail: j.siegel@io.cfmac.csic.es

FIG. 1. Laser irradiation setup (ns and fs pulses, 800 nm and 400 nm), with white light transmission and reflection micro-spectroscopy setup equipped with *in-situ* microscopy. The dashed circle contains the components necessary for 400 nm fs operation.

and alignment of the spectroscopy setup. Co-linear illumination was provided by coupling 400 nm light from a light emitting diode (LED) into the imaging path by means of a broadband non-polarizing beam splitter (NPBS). The lenses used (L2 = 200 mm and L3 = 50 mm) serve for obtaining a homogeneously illuminated field-of-view. For transmission microspectroscopy, a white light source (WLS1) was collimated to illuminate an aperture with a diameter of 100 μm (pinhole 1), which was imaged onto the front surface of the sample by means of an 80× objective lens, yielding a spot size of 4 μm.

A linear polarizer was used to set and align the polarization either along the x- or y-axis (perpendicular and parallel to the laser polarization, respectively). Care was taken to achieve a sharp image of the aperture at the sample plane with help of the *in situ* microscope, which also enabled us to position the white light probe spot onto the desired location of the irradiated area. The light transmitted through the sample was collimated by the 20× objective, reflected in part by a 50/50 metallic beam splitter towards a 10× objective lens, which coupled it into an optical fiber connected to a spectrometer.

For reflection micro-spectroscopy, WLS2 was used to illuminate pinhole 2, which was imaged by means of L2 and the 20× objective after having passed polarizer 2 for polarization control, yielding a spot size of 18 μm. The light reflected from the sample surface was collimated by the objective lens and coupled into the fiber spectrometer.

The sample used consisted of a single layer of Ag NPs embedded in a protective amorphous Al_2O_3 (a-Al_2O_3) matrix to prevent oxidation,[14] deposited on a fused silica substrate. The samples were produced by alternate PLD in vacuum from polycrystalline Al_2O_3 and Ag rotating targets. The size of the Ag NPs was selected to be near coalescence, whereas the thicknesses of the a-Al_2O_3 layers were 10 nm and 16 nm, respectively. Further details of the preparation procedure can be found elsewhere.[15]

In the first set of experiments, we studied the influence of ns laser pulses on the optical properties of the sample.

Performing a series of single pulse irradiations at increasing fluence we observed a fluence window in which a dramatic change in the reflectivity and transmission spectra was induced, indicative of a size and/or shape change of the NPs. Fig. 2 shows the results obtained for a single pulse irradiation at a peak fluence of 0.74 J/cm², which led to the strongest change without film damage.

The optical micrographs (Figs. 2(a) and 2(c)) were recorded *ex-situ* with a commercial microscope using white light illumination, a 50× (N.A. = 0.8) objective lens and a color digital camera. These color images illustrate the strong shift of the SPR induced by the laser pulse, which is quantified by the recorded spectra (Figs. 2(b) and 2(d)). The spectra shown have been normalized using the transmission and reflectivity of the fused silica substrate as reference.

In reflection, the peak wavelength measured for the as-grown film (680 nm) is blue-shifted upon irradiation to 475 nm. In transmission, an even stronger shift of the minimum down to 450 nm is observed. In both cases, the shift is accompanied by a narrowing of the spectral width and amplitude increase of the SPR, consistent with a narrowing of the size and shape distribution of the NPs. We have verified that the spectra are not sensitive to the polarization of the probe light (results shown in Fig. 4(a)). This confirms that there is no shape anisotropy, as expected due to the relatively long pulse duration and opposed to the case of irradiation with ultrashort laser pulses.[7,8,10,12]

In order to precisely determine the SPR of the sample, we have calculated the absorption spectrum from the reflectivity and transmission spectra as $A(\lambda) = 1 - R(\lambda) - T(\lambda)$.
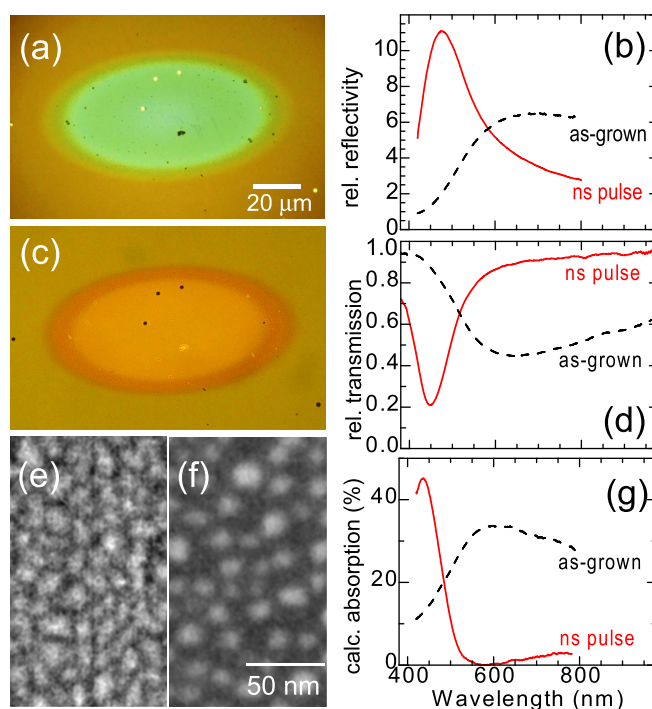
FIG. 2. (a) and (c) Color optical micrographs and (b) and (d) measured spectra of laser irradiated and as-grown regions of the sample. (a) and (b) are obtained in reflection, (c) and (d) in transmission. The absorption spectrum shown in (g) has been calculated from (b) and (d). The narrower spectral window covered in (b) and (g) is due to the spectral cut of the NPBS in Fig. 1. (e) and (f) show plan view SEM images of an as-grown and laser-irradiated sample, respectively.

We neglect scattering, which seems a reasonable assumption due to the measurement conditions used, based on microscope objective lenses with relatively high numerical apertures for high collection efficiency of scattered light. For calculating the absorbance spectrum of the embedded NP layer, the contribution of the two reflections at the two substrate interfaces had to be taken into account. The so-obtained absorption spectra for the as-grown and laser-irradiated region are shown in Fig. 2(g). They show that the as-grown film absorbs strongly over the entire visible wavelength range, featuring a very broad SPR centred at 590 nm. In contrast, after laser irradiation with a single ns laser pulse, a very pronounced narrow SPR, compared to the as-grown sample, centred at 435 nm appears, with low absorption for $\lambda > 540$ nm.

We have performed scanning electron microscopy (SEM) studies to relate the changes observed in the optical response to a modification of the NP distribution. For this purpose, the same embedded NP film was grown on a Si substrate (instead of fused silica) to avoid surface charging by the electron beam. Figs. 2(e) and 2(f) show plan view SEM images of as-grown and laser-irradiated regions, respectively. Despite the poor contrast, due to the insulating nature of the a-Al$_2$O$_3$ layer, the effect of the laser irradiation on NPs shape and distribution can be appreciated. While the as-grown film features elongated near-coalescence NPs with an average in-plane long and short axis length close to 20 and 11 nm, respectively (c.f. Fig. 2(e)), after irradiation the NPs are well-separated and have an almost circular in-plane projected shape (average diameter of 15 nm, c.f. Fig. 2(f)). The decrease in NP density from 2.5×10^3 NPs/μm^2 (as-grown film) down to 1.4×10^3 NPs/μm^2 (irradiated film) hints at the increased NP distance. This behavior is consistent with a purely thermal mechanism, involving melting up to temperatures close to the boiling point, without the initial elongation due to electron ejection/Ag-ion emission/ recombination as induced by fs laser pulses.[10,12] The larger inter-particle separation implies reduced inter-particle interactions, consistent with the experimentally observed blue-shift of the SPR.[16]

Exploiting the small size of the white light probe spot (4 μm), we have performed transmission measurements across the laser-irradiated area with a step size of 2 μm. Fig. 3 shows the data obtained in form of a map, with the horizontal axis corresponding to the position of the probe spot with respect to the center of the laser-irradiated region, the vertical axis corresponding to the wavelength of the spectra recorded, and with the corresponding transmission value encoded in a false color scale. Dark regions in the map correspond to low transmission values and are therefore a monitor of the spectral position, width and strength of the SPR. Starting from outside the laser-irradiated region (-70 μm) a gradual narrowing, shift, and amplitude increase of the initially broad SPR is observed upon moving towards the dark orange outer ring of the laser-written spot (c.f. top image of Fig. 3). The transition into the "ring" region is spectrally continuous, indicating a gradual NP size/shape/separation change of thermal origin, rather than a sudden threshold-like process as the microscope image might suggest. Moving further from the ring into the central light orange disk region is accompanied by only small spectral changes. Importantly,
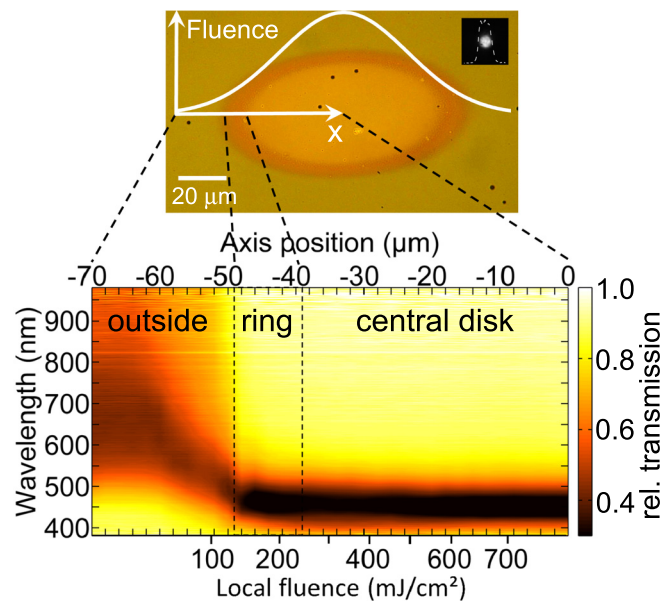

FIG. 3. (Top) Color optical transmission micrograph of the laser-irradiated area from Fig. 2(c). Superimposed is the corresponding local fluence distribution. The inset shows the measured size of the white light probe spot used for spectral measurements. (Bottom) Spectrum-fluence maps of the transmission (false color scale in percentage). The correspondence between spatial position (top axis) and local fluence (bottom axis) has been calculated. Dashed vertical lines indicate the three regimes visible in the micrograph, the light orange central disk, the dark orange ring, and the light brown outer region.

the amplitude and width of the SPR within the entire disk region is constant.

We have exploited the Gaussian spatial intensity distribution of the laser beam at the sample surface for assigning a well-defined local fluence value to each spatial position of the irradiated area. This way we could add a local fluence axis to Fig. 3, yielding a complete spectrum-fluence characterization of the transmission using only a single laser-written spot. The map covers a fluence range from the peak fluence 0.74 J/cm^2 down to 0.02 J/cm^2. This allows identifying with precision the threshold fluence for the appearance of the dark orange region (0.13 J/cm^2), corresponding to the formation of a sharp SPR.

These results demonstrate the huge potential of ns laser pulses for tailoring the optical response of embedded metal NPs, leading to stronger SPRs than achievable with fs laser pulse irradiation.[12] However, a clear advantage of fs laser pulses is their ability to generate anisotropy in the NP shape (and thus in the optical response) due to the high peak intensities, which trigger the electron emission at the poles of the NP along the laser polarization axis.[10] We have combined both techniques, ns laser irradiation to optimize the SPR in terms of amplitude and shape and subsequent fs laser irradiation to induce polarization anisotropy in the SPR. First, we have written an array of spots with single ns laser pulses at 0.74 J/cm^2, separated sufficiently to avoid pulse overlap. In the second step, we have exposed each spot to multiple fs laser pulses, since it has been reported that irradiation with tens or hundreds of low energy pulses has a stronger effect on the NP shape than a single pulse of high energy.[7,8,10,12] The fs laser fluence/pulse number was increased between different spots and the whole study was performed for fs
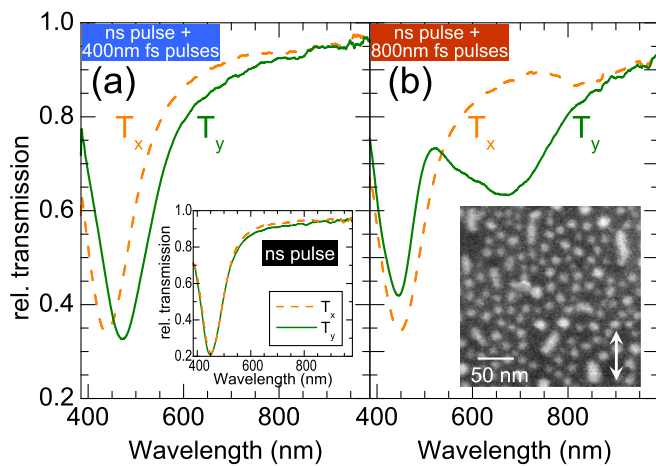
FIG. 4. Transmission spectra obtained with polarized white light of the sample exposed to a single ns laser pulse and subsequently to multiple fs laser pulses at (a) 400 nm and (b) 800 nm wavelength. T_x and T_y correspond to polarization along the x and y axis, with y being the orientation of the irradiation laser polarization. The inset in (a) shows the spectra obtained for exposure to a single ns pulse. The inset in (b) shows a plan view SEM image, with the arrow indicating the polarization direction.

laser pulses at 400 nm and 800 nm. The optimum fluence and pulse number was identified by evaluation of the SPR in terms of amplitude and polarization anisotropy in each case. We observed that the higher the pulse number or fluence, the stronger is the induced spectral shift/anisotropy and that the higher the fluence the lower is the pulse number required to reach a certain shift.

Fig. 4(a) shows the results for 200 pulses at 400 nm and a fluence of 0.11 J/cm^2, featuring a relatively small but significant polarization anisotropy with a peak shift of $\Delta\lambda_{anisotropy} = 35$ nm. The component parallel to the laser polarization (T_y) is red-shifted due to a slight elongation of the NPs along this direction. Such small shape anisotropy would likely be missed in SEM or TEM studies but shows up in optical characterization due to its ability to resolve small but systematic changes of the SPR.

For post-irradiation with 800 nm fs laser pulses, a different type of anisotropy is observed as can be seen in Fig. 4(b), showing the results for 40 pulses at 0.28 J/cm^2. Here, the T_y spectrum appears bimodal, which is most likely related to a bimodal shape distribution of the NPs. Such bimodal shape distribution can indeed be appreciated in the SEM image of a laser-irradiated region (inset of Fig. 4(b)), featuring some elongated NPs aligned along the direction of the laser polarization within a distribution of spherical NPs. The strong spectral shift of the second mode ($\Delta\lambda_{anisotropy} = 230$ nm) indicates a relatively large aspect ratio of the prolate spheroids formed, which is consistent with previous studies of NPs embedded in bulk glass.[8] We attribute this larger shift to off-resonance excitation, favoring field-enhancement in the particle vicinity and field-driven electron ejection. In view of the SEM image, we speculate that this process causes some neighbor particles to join and form long chains. In contrast, for resonant excitation (400 nm) enhanced absorption leads to less anisotropy due to stronger thermal effects.[12]

In conclusion, we have reported optical spectrum tailoring of a monolayer of *embedded* Ag NPs based on particle shape changes using *ns* laser pulses. The underlying mechanisms are thermal in nature, leading to a change in shape and separation. The large spectral shift and narrowing of the SPR relates to the formation of a homogeneous distribution of well-separated, spherical NPs, as supported by SEM images. The complete optical characterization in terms of transmission and reflectivity allows the determination of the absorption spectra, which is a direct monitor of the SPR. Spectral mapping with high spatial resolution combined with Gaussian intensity distribution allows for a precise determination of the fluence threshold for this process. Hybrid processing with ns and fs laser pulses provides the benefit of generating a strong SPR and polarization anisotropy in the optical response. This approach offers excellent perspectives for optical encoding,[17,18] and fabrication of complex, polarization-sensitive spectral masks starting from thin films with random distributions of NPs.

[1] U. Kreibig and M. Vollmer, *Optical Properties of Metal Clusters* (Springer Verlag, Berlin, 1995).
[2] D.-Q. Yang, M. Meunier, and E. Sacher, J. Appl. Phys. **95**, 5023 (2004).
[3] V. Resta, J. Siegel, J. Bonse, J. Gonzalo, C. N. Afonso, E. Piscopiello, and G. Van Tenedeloo, J. Appl. Phys. **100**, 084311 (2006).
[4] A. Nicolas Filippin, A. Borras, V. J. Rico, F. Frutos, and A. R. Gonzalez-Elipe, Nanotechnology **24**, 045301 (2013).
[5] D. Babonneau, S. Camelio, L. Simonot, F. Pailloux, P. Guérin, B. Lamongie, and O. Lyon, Europhys. Lett. **93**, 26005 (2011).
[6] E. Fort, C. Ricolleau, and J. Sau-Pueyo, Nano Lett. **3**, 65 (2003).
[7] M. Kaempfe, T. Rainer, K.-J. Berg, G. Seifert, and H. Graener, Appl. Phys. Lett. **74**, 1200 (1999); **77**, 459 (2000).
[8] A. Stalmashonak, C. Matyssek, O. Kiriyenko, W. Hergert, H. Graener, and G. Seifert, Opt. Lett. **35**, 1671 (2010).
[9] A. Stalmashonak, H. Graener, and G. Seifert, Appl. Phys. Lett. **94**, 193111 (2009).
[10] A. Stalmashonak, A. Podlipensky, G. Seifert, and H. Graener, Appl. Phys. B **94**, 459 (2009).
[11] A. Akin Unal, A. Stalmashonak, G. Seifert, and H. Graener, Proc. SPIE **7032**, 703225 (2008).
[12] G. Baraldi, J. Gonzalo, J. Solis, and J. Siegel, Nanotechnology **24**, 255301 (2013).
[13] J. M. Liu, Opt. Lett. **7**, 196 (1982).
[14] G. Baraldi, M. Carrada, J. Toudert, F. J. Ferrer, A. Arbouet, V. Paillard, and J. Gonzalo, J. Phys. Chem. C **117**, 9431 (2013).
[15] J.-P. Barnes, A. K. Petford-Long, R. C. Doole, R. Serna, J. Gonzalo, A. Suarez-Garcia, C. N. Afonso, and D. E. Hole, Nanotechnology **13**, 465 (2002).
[16] Z. Liu, H. Wang, H. Li, and X. Wang, Appl. Phys. Lett. **72**, 1823 (1998).
[17] A. Siozios, D. C. Koutsogeorgis, E. Lidorikis, G. P. Dimitrakopulos, Th. Kehagias, H. Zoubos, Ph. Komninou, W. M. Cranton, C. Kosmidis, and P. Patsalas, Nano Lett. **12**, 259 (2012).
[18] P. Zijlstra, J. W. M. Chon, and M. Gu, Nature **459**, 410 (2009).